

is subjected to base acceleration  $F(t)$  having a zero mean and power spectral density (PSD)  $\phi_{FF}(f)$  shown in Fig. 1. The optimization problem is stated as: Minimize-Weight Function:

$$W(\bar{D}) = \rho(d_1 l_1 + d_2 l_2)$$

subject to stress constraint

$$P \left[ \bigcup_{i=1}^2 \left\{ |s_i(t)| \geq r \right\} \right] \leq 10^{-3}$$

Frequency constraint

$$10 \leq f_1 \leq 15, \quad f_2 \geq 20$$

where  $s_i$ ,  $i = 1, 2$  is stress in the  $i$ th bar,  $r$  is the random yield stress with mean  $\mu_R = \pm 20 \times 10^3$  psi and standard deviation  $\sigma_R = 3 \times 10^3$  psi.  $F(t)$  and  $Y$  are assumed to be independent and Gaussian. Mean and Variance of the stresses is obtained using the frequency domain approach. Since the problem has only two design variables, optimum design is obtained graphically as shown in Fig. 1.

Note that the frequency constraint is specified such that the natural frequencies of the system lie in regions where  $\phi_{FF}(f)$  has small values and is flat. This has the effect of reducing the response and thereby leading to a better design. Also since the spectral density is flat in the region of interest, calculations can be simplified by the white noise assumption for lightly damped structures.<sup>2</sup>

2) Cantilever with Tip Mass—A cantilever beam with thin-walled box section and a tip mass, shown as inset in Fig. 2, is subjected to a base acceleration  $F(t)$  with zero mean and PSD  $\phi_{FF}(f)$  as shown in Fig. 2. The optimization problem is stated as: Minimize—Expected Rate of Fatigue Damage<sup>2</sup>

$$ED(\bar{D}) = \frac{N_0^+}{\beta} [(2)^{1/2} \sigma_s]^2 \Gamma(1 + \alpha/2)$$

subject to stress constraint

$$P [|s(t)| \geq r] \leq 10^{-3}$$

acceleration constraint

$$P [|a(t)| \geq 10g] \leq 10^{-3}$$

weight constraint

$$W/\rho l \leq 10$$

frequency constraint

$$f \geq 10$$

where  $N_0^+$  is the number of zero crossings with positive slope,  $\alpha = 6.0$ ,  $\beta = 6.4 \times 10^{31}$  are coefficients in the assumed law of fatigue failure ( $Ns^\alpha = \beta$ ),  $s$  is the maximum stress at the root of the cantilever,  $r$  is the yield stress with mean  $\mu_R = \pm 18 \times 10^3$  psi and  $\sigma_R = 2 \times 10^3$  psi,  $a$  is the absolute acceleration of the tip mass,  $W$  is the weight of the beam, and  $f$  is the fundamental frequency of the system in cps. Response calculations have been carried in the frequency domain assuming the beam to be weightless. Thickness of the beam was assumed to be constant and equal to  $t = 0.2$  in., tip mass  $m = 1.0$  and viscous damping  $\zeta = 0.02$ . Since thickness is assumed to be constant, the problem has two design variables, width  $b$  and depth  $d$ . Graphical solution (Fig. 2) gives the optimum design:  $b = 15$  in.,  $d = 10$  in. and  $t = 0.2$  in. with objective function  $ED = 1.0 \times 10^{-8}$ .

The problem was also solved for three design variables  $b$ ,  $d$ ,  $t$  using unconstrained minimization technique. The optimum design is obtained for  $b = 36.62$  in.,  $d = 9.2$  in. and  $t = 0.108$  in. with  $ED = 0.645 \times 10^{-8}$ , giving a reduction of 35.5% over previous design.

## Conclusions

The optimization problem with probabilistic constraints on the dynamic response of a system can be transformed to a standard nonlinear programming problem and solved by any of the well-known methods. Constraints on the natural frequencies of the system are both important and convenient in such problems. Power spectral density curves provide a direct visual basis for choosing these constraints.

## References

- Shinozuka, M., "Probability of Structural Failure Under Random Loading," *Engineering Mechanics Division Journal*, ASCE, Vol. 90 (EM5), 1964, pp. 147-170.
- Lin, Y. K., *Probabilistic Theory of Structural Dynamics*, 1st ed. McGraw-Hill, New York, 1967, chaps. 5 and 9.

## Effects of Transverse Outflow from a Hypersonic Separated Region

ALLEN H. WHITEHEAD JR.,\* JAMES R. STERRETT,†

AND JAMES C. EMERY‡

NASA Langley Research Center, Hampton, Va.

THE design of hypersonic configurations such as the space-shuttle must consider the consequences of separated flows over protrusions, control surfaces or ahead of jet-interaction controls. These flows will be characterized by transverse-relief effects. Particularly in the critical region around reattachment where the pressure and heating are experimentally and theoretically important, data are extremely limited, and no hypersonic studies can be found to indicate the effect of a systematic variation in transverse outflow on conditions at the reattachment point even over nominally two-dimensional geometries. Recent reviews of the separation problem (for example, Ref. 1) recognize that the pressure rise at reattachment provides a closure condition in the analysis which is as important as the separation point and the separated shear layer in determining the structure and properties of the separated flow region. Most theoretical models do not account for transverse outflow effects, but assume as in the Chapman<sup>2</sup> approach that fluid escapes the separated region only through mixing across the separated shear layer. The present study examines features of hypersonic, finite-span separated flows with a turbulent boundary-layer to provide a partial assessment of transverse-outflow effects on separated flowfield characteristics.

An illustration of three-dimensional separated flows is given in Fig. 1 which shows an unpublished oil flow photograph of the canopy region of a straight-wing shuttle orbiter (from an investigation reported in Ref. 3). A clearly identified reattachment occurs as well as extensive transverse flow from the reverse-flow region. Other regions on this orbiter also exhibit three-dimensional separation. To provide a preliminary assessment of such outflow effects, studies were conducted on variable-span, forward-facing steps and wedges ( $\bar{w}$  = ratio of model span to full-span step or wedge) in the Langley 20-in. Mach 6 Tunnel at a unit Reynolds number of 21 million/m (6.4 million/ft). The span of the plate was 25 cm, and the distance from the leading edge to the step or wedge was 39.4 cm. The constant step height of 2.92 cm ( $h$ ) was about five times the boundary-layer thickness just upstream of separation; the 40° wedges had a slant length ( $h$ ) of 10.6 cm. From criteria developed by Morrisette et al.,<sup>4</sup> roughness elements placed 5.0 cm from the plate leading edge assured a well developed turbulent boundary-layer prior to separation. Oil flow studies were used to locate separation and reattachment.

Received November 15, 1971.

\* Aerospace Engineer, Configuration Flow Fields Section. Associate AIAA.

† Head, Configuration Flow Fields Section. Member AIAA.

‡ Aerospace Engineer, Configuration Flow Fields Section.

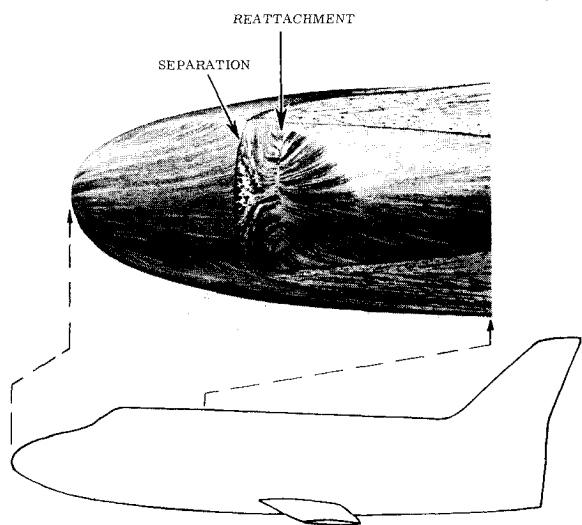


Fig. 1 Oil-flow pattern over straight-wing shuttle orbiter at zero angle of attack.  $M_\infty = 6.0$ ;  $R/m = 16 \times 10^6$ .

A significant influence of model span on the center line pressure distribution on the faces of the step and wedge flows was found as shown in Fig. 2. The face pressures ( $p$ ) in this figure are normalized by the freestream static pressure ( $p_\infty$ ). Oil flow results indicate that reattachment occurs just below the top corner of the forward-facing step regardless of the model span. Thus, the data point at  $y/h = 0.96$  in Fig. 2a is the approximate reattachment pressure and the assumed peak value. On a similar full span step in a turbulent boundary-layer flow at Mach 4.0, Behrens<sup>5</sup> found reattachment at about  $y/h = 0.97$ . End or transverse-outflow effects are present even for the full-span step in the present tests as illustrated by Fig. 2a; when the end plates are removed, the reattachment pressure doubles. With the full-span step replaced by the half-span model ( $\bar{w} = 0.5$ ), only a 20% increase occurs in the reattachment pressure. A further reduction in the span to  $\bar{w} = 0.2$  results in a significant change in the face pressure distribution with a reattachment pressure four times the full-span value. Whereas the variation in  $h/w$  for these tests was obtained by changing step span ( $w$ ), the change in this parameter in the tests reported in Ref. 6 was achieved by altering the height ( $h$ ) of a full-span step. These data shown in Fig. 2c were also obtained in the 20-in. Mach 6 facility under turbulent boundary-layer conditions. Note that the reattachment pressure ratio varies from 9–70 as a result of a variation in  $h/w$  from 0.04 to 0.58. The probable explanation for this behavior is that increasing the transverse outflow by decreasing  $w$  (or increasing  $h$ ) causes a greater mass of fluid to be turned down the face below the dividing streamline; then as suggested in the sketch in Fig. 2, the shear-layer velocity profile is lowered relative to the dividing streamline and a higher energy portion of the shear layer impinges on the step face. A similar reasoning was employed in Zukoski's<sup>7</sup> analysis of outflow effects from a full-span step without end plates. A maximum reattachment pressure calculated assuming a two-shock flow model is shown in Fig. 2c. In this calculation the strength of the oblique separation shock is obtained from the empirical plateau-pressure relation of Sterrett<sup>8</sup> followed by a normal bow shock.

The oil flow and pressure distribution on the faces of the 40° deflected wedges in Fig. 2 show significant differences from the data obtained on the forward-facing steps: 1) on the wedges, reattachment occurs on the lower half of the wedge face, and the pressure peak occurs a considerable distance downstream of reattachment. The peak and reattachment location on the step are nearly coincident at the top corner. 2) Whereas the step reattachment pressure increases sharply with  $h/w$ , the peak and reattachment pressures on the wedge face indicate a slight decrease with this parameter. 3) The separation distances measured upstream from the corner ( $x_s$ ) are nearly constant for changing step span (Fig. 2d). In contrast, decreasing the span of the wedge significantly shrinks the separation region. These characteristic differences in response to changing span are

probably attributable to the nature of the reattachment process; that is, the reattachment point is fixed on the step face, but is free to seek a location satisfying fluid-dynamic equilibrium criteria on the wedge model. Since the type of reattachment ("fixed" or "free") determines the magnitude and location of the peak pressure (and peak heating) and since these peaks could be a design factor in the development of hypersonic vehicles, it would be desirable to discover the criteria that determines whether an increase in transverse outflow will result in a free or a fixed reattachment. This study suggests that the angle of a protuberance with the flow is a key factor; obviously, the protuberance height and span relative to the undisturbed boundary-layer thickness are also important factors in the determination of the type of reattachment. For example, if a step height is sufficiently large compared to the unseparated boundary-layer thickness, the reattachment will occur well below the corner and a free reattachment could result.

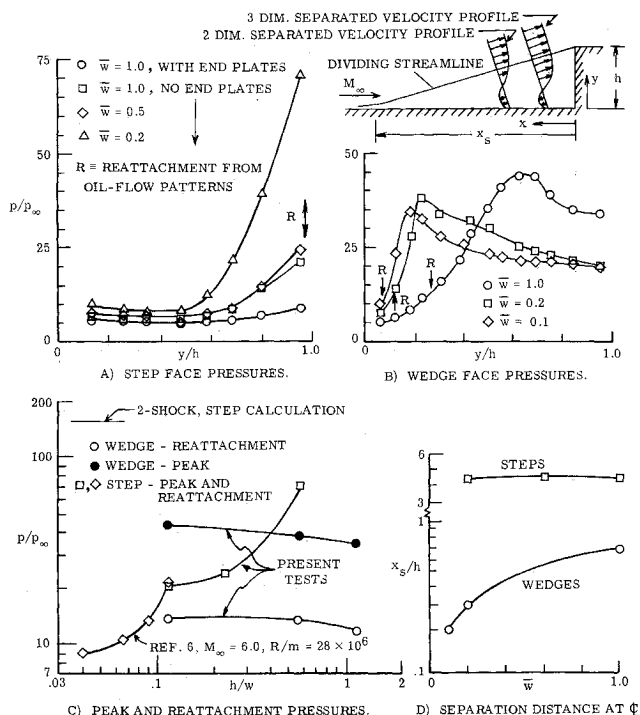


Fig. 2 Centerline face-pressure distributions and separation distances.  $M_\infty = 6.0$ ;  $R/m = 21 \times 10^6$ .

To further develop the understanding of the flow over the face of the steps and wedges, a total-head probe was introduced into the flow from a base plate ahead of the corner. The probe was maintained parallel to the face at the center line, and was moved from the reattachment point to the bottom corner of the step or wedge at different stations off the model face. These Pitot pressures were then combined with the static pressures measured on the face to yield a Mach number distribution in the flowfield. The assumption of a constant static pressure across the flow moving down the face was checked by placing a static pressure probe at a distance of 0.15 cm ( $x/h = 0.05$ ) from the step face at  $y/h = 0.5$ . The static pressure obtained in the flowfield was only slightly lower than that measured on the face. The Mach number distribution just off the model face is shown in Fig. 3a for the three steps and the full-span wedge where  $y_R$  is the distance from the bottom corner to the reattachment location. The flow down the wedge gradually increases in velocity, but never attains the Mach number levels found on the steps. The Mach number down the face of the step increases to a supersonic maximum around the midheight station and then falls off rapidly. Increasing the extent of lateral outflow down the face increases the over-all magnitude of the local Mach number, a plausible result since the driving potential for this flow is controlled by an increasing reattachment pressure.

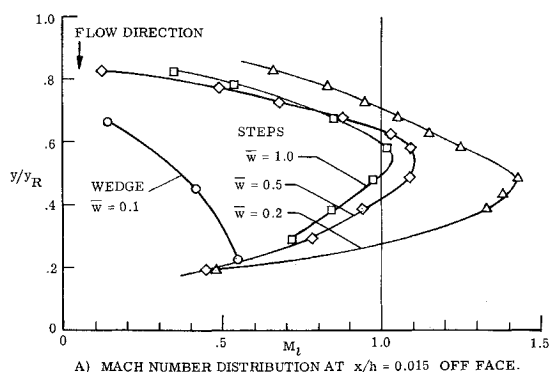
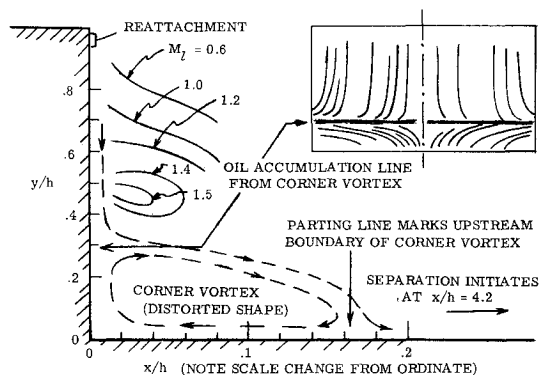
A) MACH NUMBER DISTRIBUTION AT  $x/h = 0.015$  OFF FACE.B) FLOW-FIELD CONTOURS AND OIL-FLOW TRACING FOR  $\bar{w} = 0.2$  STEP.

Fig. 3 Mach number distribution down faces of wedges and steps.  
 $M_\infty = 6.0$ ;  $R/m = 21 \times 10^6$ .

Oil flow results from the  $\bar{w} = 0.2$  step face shown in Fig. 3b (obtained from a tracing of the photograph) identified a local vortex flow in the bottom corner of the step. The flow up the face from the corner is then opposed by the flow moving down the face from reattachment, resulting in an oil accumulation line located near  $y/h = 0.3$  for the  $\bar{w} = 0.2$  step. This secondary vortex was observed in the corners of all steps in this investigation and also in the tests reported by Behrens.<sup>5</sup> Mach number contours obtained from probe surveys at stations off the  $\bar{w} = 0.2$  step face are sketched in Fig. 3b (note that the horizontal and vertical scales are dissimilar). A considerable portion of this flow down the face is found to be supersonic. A shock system is probably required in the neighborhood of the oil accumulation line to decelerate the flow as it approaches the corner.

The present study has shown the critical importance of transverse outflow in determining some of the characteristic features of a turbulent, separated boundary layer. Continued refinements in two-dimensional analytical methods which do not account for transverse-outflow effects are of limited benefit to the designer of hypersonic vehicles who must be concerned with finite-span separations. Mach number profiles when considered with oil flow patterns permit an elementary modeling of the reverse flow region adjacent to the face of a forward-facing step with transverse outflow.

### References

- 1 Roshko, A., "Review of Concepts in Separated Flow," *Canadian Congress of Applied Mechanics*, edited by B. H. Karnopp of Toronto, Vol. 3, May 1967, pp. 3-81 to 3-115.
- 2 Chapman, D. R., Kuehn, D. M., and Larson, H. K., "Investigation of Separated Flows in Supersonic and Subsonic Streams With Emphasis on the Effects of Transition," Rept. 1356, 1958, NACA.
- 3 Hefner, J. N., and Whitehead, A. H. Jr., "Lee-Side Heating Investigations: Part I—Experimental Lee-Side Heating Studies on a Delta-Wing Orbiter," TM X-2272, March 1971, NASA.
- 4 Morrisette, E. L., Stone, D. R., and Whitehead, A. H., Jr., "Viscous Drag Reduction," *Boundary Layer Tripping With Emphasis on Hypersonic Flows*, edited by C. S. Wells, Plenum Press, N.Y., pp. 33-51.
- 5 Behrens, W., "Separation of a Supersonic Turbulent Boundary Layer by a Forward Facing Step," AIAA Paper 71-127, New York, 1971.

<sup>6</sup> Sterrett, J. R. and Barber, J. B., "A Theoretical and Experimental Investigation of Secondary Jets in a Mach 6 Free Stream With Emphasis on the Structure of the Jet Separation Ahead of the Jet," *Proceedings of the Agard Conference 4, Separated Flows, Part II*, May 1966, pp. 667-700.

<sup>7</sup> Zukoski, E. E., "Turbulent Boundary-Layer Separation in Front of a Forward-Facing Step," *AIAA Journal*, Vol. 5, No. 10, Oct. 1967, pp. 1746-1753.

<sup>8</sup> Sterrett, J. R. and Emery, J. C., "Extension of Boundary-Layer Separation Criteria to a Mach Number of 6.5 by Utilizing Flat Plates With Forward-Facing Steps," TN D-618, Dec. 1960, NASA.

## Impact Probe Displacement in a Supersonic Turbulent Boundary Layer

JERRY M. ALLEN\*

NASA Langley Research Center, Hampton, Va.

### Nomenclature

- $D$  = impact probe outside diameter  
 $M$  = Mach number  
 $M_e$  = boundary-layer edge Mach number  
 $Y$  = distance normal to test surface  
 $\delta$  = boundary-layer thickness  
 $\Delta$  = impact probe displacement

### 1. Introduction

IMPACT pressure measurements in boundary-layer research are usually performed with probes which are very small relative to the boundary-layer thickness in order to minimize any influences of probe size on the resulting measurements. When this is not possible, and the experimenter wants to correct his measurements for probe displacement effects, the works of Young and Maas<sup>1</sup> and MacMillan<sup>2</sup> are available for incompressible wakes and incompressible turbulent boundary layers, respectively. A literature search, however, revealed that no comparable work has been performed in a supersonic turbulent boundary layer. The bow shock wave ahead of an impact probe in supersonic flow could significantly affect the displacement compared to the incompressible case. This study was thus undertaken to provide experimental impact probe displacement results in a two-dimensional supersonic turbulent boundary layer.

### 2. Experiment

The experiment was performed on the test section sidewall in Langley's 4-ft  $\times$  4-ft supersonic pressure tunnel.<sup>3</sup> The nominal freestream Mach number of 2.0, stagnation pressure of 0.69 atm, and stagnation temperature of 41°C resulted in a unit Reynolds number of about  $8 \times 10^6/m$  and a Reynolds number based on the distance from the tunnel throat to the survey station of about  $43 \times 10^6$ .

The boundary layer at the test station was surveyed in turn by each of 8 impact probes ranging in size from about 1.3 to 48 mm. This largest probe was about 70% of the boundary-layer thickness. The probes were circular in cross section and had inside-to-outside diameter ratios of about 0.6. The impact pressures measured by these probes were combined with the test section static pressure to calculate Mach numbers. Probe displacement effects were evaluated in terms of these Mach number values.

### 3. Discussion

Figure 1 shows the probe Mach number variations with probe diameter. The curves connect points of constant  $Y$ ; that is, points whose probe centers are located at the same position in the boundary layer. The extrapolation of these curves to  $D = 0$  should give the true Mach number profile for this boundary layer.

Received November 19, 1971.

\* Aerospace-Technologist, High-Speed Aircraft Division. Member AIAA.